A DFT Perspective on the Structures and Electronic Spectra of the Orange and Blue Isomers of Photochromic Dithizonatophenylmercury(II)

Karel G. von Eschwege, Jeanet Conradie,* and Jannie C. Swarts

Department of Chemistry, PO Box 339, University of the Free State, Bloemfontein, 9300, South Africa

Received: August 29, 2007; In Final Form: December 18, 2007

The molecular structure and electronic spectra of the orange and blue isomers of the photochromic compound dithizonatophenylmercury(II) were theoretically studied utilizing density functional (DFT) methods. Computed structural results are in agreement with previously reported X-ray crystal data of the orange resting state. The herewith newly proposed geometrical structure of the blue photoexcited state is favored by more than 35 kJ·mol^{-1} relative to the historically hypothesized geometry of the blue isomeric form. The key difference lies in the position of the backbone amine proton, being situated on the N4 position in the newly proposed structure, rather than on the N2 position as in the previously *hypothesized* geometry. Time dependent density functional theory as implemented in the Amsterdam Density Functional (ADF) and Gaussian 03 (G03) program systems yielded excitation energies for the blue isomer exhibiting bathochromic shifts, as observed in the experimentally determined UV/visible spectrum. B3LYP calculated excitation energies and oscillator strengths gave the best approximation of the experimentally observed electronic spectra of both isomers.

1. Introduction

Between 1945 and 1950 photochromism of mercury(II) dithizonato complexes was independently discovered and reported by Reith and Gerritsma,[1] Irving and co-workers,[2] and Webb and co-workers.[3] In 1965 Meriwether and co-workers prepared 24 metal dithizonates, of which nine were found to be photochromic in visible light.[4] Half-lives of the photoexcited states of the different metal complexes in nonpolar solvents such as benzene and chloroform varied from less than 1 s to more than 60 s for the mercury complex, at 25 °C.[4] The proposed photochromic reaction (Scheme 1) entails photoisomerization of the orange mercury(II) dithizonate complex to the blue form, followed by a spontaneous radiationless thermal back reaction.[5]

The structure of the orange isomer was confirmed by X-ray crystallography.[6] On the other hand, the proposed geometry of the blue form, as indicated in Scheme 1, had to date been accepted without proper validation. Meriwether provided infrared spectroscopic evidence for the replacement of a stronger S−H hydrogen bond in the orange form by a weaker hydrogen-bonded −NH group in the activated form upon radiation. Due to observed rapid deuterium exchange in the complex, and increased back reaction rates under altered pH conditions or the presence of polar solvent molecules like water, it was hypothesized that intermolecular proton transfer from N4 to N2 may take place, albeit, not directly. It was suggested that a water molecule or a second molecule of complex, or both, serves as a proton bridge, with the activated complex probably consisting of several water and dithizonate molecules bound together by hydrogen bonds. It was nevertheless also noted that both the forward and back reactions do take place in dry benzene as well.[7] Several polymers containing the still active photochromic moiety were also prepared.[8] However, when the mercury dithizonate complex is encapsulated inside the polymer, water and other protic species are excluded from taking part in the photochromic reaction. Free diffusion of the polymer-bound photochromic moiety is also not possible. The fact that photochromism was still observed in these polymers contradicts the previously proposed intermolecular proton exchange mechanism.

SCHEME 1: The Structure of the Ground State Orange Isomer (a) of Photochromic Dithizonatophenylmercury(II) Was Confirmed by X-ray Analysis, but the Hypothesized Structure of the Light-Excited Blue Isomer (b) Was Never Validated

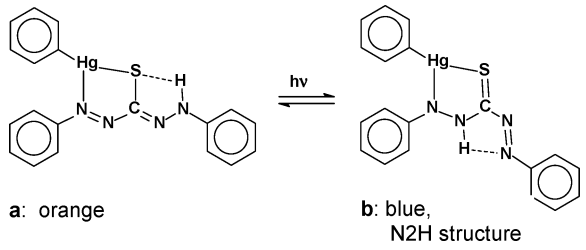

The above-described observations and the absence of crystal data for the blue form led us to reinvestigate both the structures and mechanism involved in the photochromic reaction of dithizonatophenylmercury(II). The lack of crystallographic data of the blue form made a quantum computational study the method of choice to better substantiate a proposed geometry for the blue isomer.

2. Experimental and Computational Methods

General. Reagent chemicals and solvents were purchased from Sigma-Aldrich and used without further purification. ^{1}H NMR spectra were recorded on a 300 MHz Bruker Avance DPX NMR spectrometer, at 298 K. Chemical shifts are reported relative to $SiMe_4$ at 0 ppm. Ultraviolet and visible spectra of dithizonatophenylmercury(II) were recorded from dilute solutions [1.5×10^{-5} M] in quartz cuvettes, utilizing a Varian Cary 50 Probe UV/visible spectrophotometer.

Synthesis. The following simplified method was used for the preparation of dithizonatophenylmercury(II).[6]

* Author to whom correspondence should be addressed. E-mail: conradj.sci@ufs.ac.za. Tel: 27-51-4012194. Fax: 27-51-4446384.

10.1021/jp076924r CCC: $40.75
Published on Web 02/15/2008

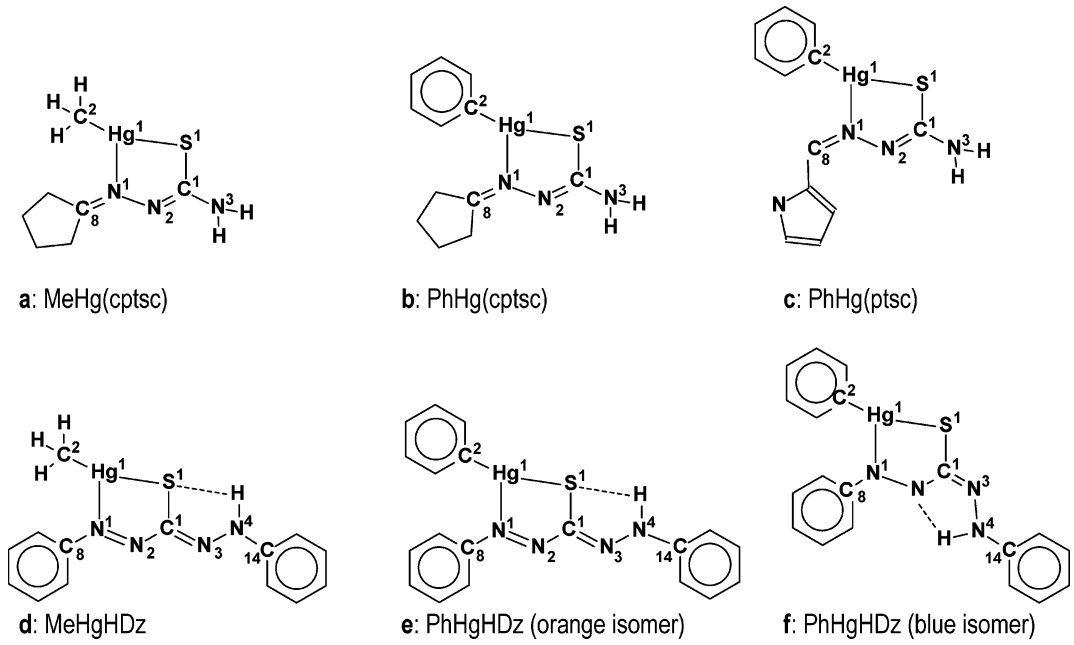

Figure 1. Structures of (a) MeHg(cptsc), (b) PhHg(cptsc), and (c) PhHg(ptsc), (d) MeHgHDz, (e) PhHgHDz (orange isomer), and (f) PhHgHDz (blue isomer), indicating atom numbering.

Triethylamine (0.51 g, 5 mmol) was added to a solution of dithizone (1.025 g, 4 mmol) and phenylmercury(II) chloride (1.315 g, 4.2 mmol) in dichloromethane (300 mL). After stirring for 15 min the solvent was removed under reduced pressure. Recrystallization of crude dithizonatophenylmercury(II) was done from dichloromethane and ethanol mixtures in an initial ratio of 3:2, to liberate 1.98 g (93%) of pure product. Mp: 166 °C. UV/vis (hexane): $\lambda_{max} = 265$ nm ($\epsilon = 32\,200$ dm^3 mol^{-1} cm^{-1}) and 471 nm ($\epsilon = 57\,300$ dm^3 mol^{-1} cm^{-1}). ^{1}H NMR (300 MHz, $CDCl_3$): δ 7.60−8.00 (3 × m, 15 H, C_6H_5).

Photoisomerization of the orange mercury complex dissolved in hexane, to the blue isomer, was conveniently induced by direct sunlight (spectral radiation maxima at *ca.* 460−560 nm), or by irradiation with an Osram Powerstar HQI-T 400 W mercury halide lamp (spectral radiation maxima at *ca.* 350−650 nm). (See Supporting Information for Solar and Osram lamp spectral distributions.)

Quantum Computational Methods. All ADF (Amsterdam Density Functional) calculations were carried out using DFT (Density Functional Theory)[9] with the PW91 (Perdew−Wang, 1991) exchange and correlation functional.[10] As a check on the performance of the PW91 functional, the OLYP[11] (OPTX exchange functional[11] combined with the Lee−Yang−Parr correlation functional[12]) GGA (Generalized Gradient Approximation) was also used for all the geometry optimizations. The ZORA[13] (Zero-Order Regular Approximation)/TZP (Triple ζ polarized) basis set including scalar relativistic effects, a fine mesh for numerical integration, a spin-unrestricted (gas-phase) formalism and full geometry optimization with tight convergence criteria as implemented in the ADF (2006) program, was used. TDDFT,[14] Time-Dependent Density Functional Theory, implemented in the ADF program was used for calculation of excitation energies. Calculations in solution, as contrasted to the gas phase, were done using the Conductor-like Screening Model (COSMO)[15] of solvation as implemented in ADF.[16]

The Gaussian full geometry optimization was done with tight convergence criteria as implemented in the Gaussian program package, version 03,[17] using the B3LYP[18] (B3 Becke 3-parameter exchange and Lee−Yang−Parr correlation) functional for both exchange and correlation, and the CEP-31G[19] (Stevens/Barch/Krauss effective core potential triple-split) basis set. Excited state energy calculations were done using the time-dependent DFT method (TD method)[20] implemented in the G03 program.

Whether artificially generated atomic coordinates, or coordinates obtained from X-ray crystal data (Cambridge Crystallographic Database) were used in the input files, optimizations for each compound resulted in the same optimized geometry. The accuracy of the different computational methods was evaluated by comparing the root-mean-square deviations (rmsd's) between the optimized molecular structure and the crystal structure, using only non-hydrogen atoms in the backbone of the molecules (phenyl, pyrrole and cyclopentane carbons excluded). Rmsd values were calculated using the "RMS Compare Structures" utility in ChemCraft Version 1.5.[21]

No symmetry limitations were imposed in the calculations.

3. Results and Discussion

Structural Investigation. Orange Isomer. Since quantum computational methods are for the first time applied to metal dithizonates and reported here, some measure of the reliability of the approach had to be obtained. This was first of all addressed by theoretically computing the structures of the orange form of dithizonatophenylmercury(II) (PhHgHDz), and comparing the calculated data with known single-crystal X-ray diffraction structural data of PhHgHDz.[6] Toward a broader foundation for computational structure accuracy, the known structures of dithizonatomethylmercury(II) (MeHgHDz),[6] cyclopentanonethiosemicarbazonato-N^3,S methylmercury(II) (MeHg(cptsc)),[22] cyclopentanonethiosemicarbazonato-N^3,S phenylmercury(II) (PhHg(cptsc))[23] and phenylpyrrole-2-carbaldehydethiosemicarbazonato-N^3,S mercury(II) (PhHg(ptsc))[23] were also computed and compared with the X-ray results. These mercury(II) compounds are all related by their 5-membered backbone rings which have similar elemental arrangements. The structural drawings of these compounds are displayed in Figure 1, with selected bond lengths and bond angles given in Tables 1 and 2.

Gas-phase calculations generally give longer bond lengths than corresponding crystal structure bond distances.[24] For

TABLE 1: Selected X-ray Crystallographic and Quantum Computational Bond Lengths (Å) and Bond Angles (deg) of Mercury Thiosemicarbazonato Compounds[a]

	MeHg(cptsc)				PhHg(cptsc)				PhHg(ptsc)			
program:		ADF	ADF	Gaussian		ADF	ADF	Gaussian		ADF	ADF	Gaussian
method:		DFT	DFT	DFT		DFT	DFT	DFT		DFT	DFT	DFT
functional:		PW91	OLYP	B3LYP		PW91	OLYP	B3LYP		PW91	OLYP	B3LYP
basis set:	X-ray	ZORA/TZP	ZORA/TZP	CEP-31G	X-ray	ZORA/TZP	ZORA/TZP	CEP-31G	X-ray	ZORA/TZP	ZORA/TZP	CEP-31G
rmsd[b]		0.08	0.10	0.13		0.13	0.13	0.20		0.05	0.06	0.09
Bond Lengths/Å												
Hg1−S1	2.380	2.427	2.422	2.507	2.382	2.422	2.414	2.497	2.377	2.427	2.423	2.509
Hg1−C2	2.088	2.118	2.117	2.151	2.063	2.101	2.101	2.128	2.048	2.096	2.098	2.124
Hg1−N1	2.539	2.592	2.722	2.562	2.489	2.584	2.711	2.544	2.492	2.546	2.649	2.501
N1−N2	1.387	1.375	1.373	1.427	1.404	1.375	1.373	1.427	1.400	1.371	1.367	1.423
N1−C8	1.259	1.289	1.292	1.312	1.264	1.291	1.292	1.312	1.283	1.308	1.308	1.329
N2−C1	1.299	1.307	1.304	1.329	1.302	1.306	1.303	1.328	1.304	1.313	1.311	1.335
C1−S1	1.753	1.779	1.779	1.849	1.751	1.780	1.780	1.851	1.742	1.770	1.771	1.841
C1−N3	1.350	1.378	1.384	1.388	1.349	1.378	1.384	1.387	1.361	1.376	1.382	1.386
Bond Angles/deg												
Hg1−S1−C1	103.0	101.4	103.1	99.9	101.4	101.3	103.0	99.7	102.4	101.2	102.4	99.5
S1−Hg1−N1	75.0	75.8	74.3	76.8	75.7	75.9	74.7	77.2	75.8	76.0	74.8	77.0
N1−Hg1−C2	117.0	116.8	116.7	119.1	120.3	118.9	117.6	119.6	118.4	116.4	116.2	118.2
Hg1−N1−N2	117.0	115.3	112.7	117.2	115.5	115.2	112.7	117.2	117.5	116.3	114.7	118.7
N1−N2−C1	114.0	116.3	117.0	116.1	114.4	116.4	117.2	116.1	113.4	116.1	116.4	115.4
N2−C1−S1	130.0	130.9	131.8	130.0	129.2	130.8	131.7	129.9	130.5	130.3	131.1	129.4
S1−C1−N3	111.0	112.8	112.2	113.1	114.0	112.8	112.2	113.1	112.3	113.0	112.6	113.4

[a] The root-mean-square deviations (rmsd) of computed structures are given. [b] Rmsd values, in angstroms, are root-mean-square atom positional deviations, calculated for non-hydrogen atoms (phenyl, pyrrole and cyclopentane carbons excluded) for the best three-dimensional superposition of calculated structures on experimental structures.

TABLE 2: Selected X-ray Crystallographic and Quantum Computational Bond Lengths (Å) and Bond Angles (deg) of Mercury Dithizonato Compounds[a]

	MeHgHDz				PhHgHDz (orange)				PhHgHDz (blue)		
program:		ADF	ADF	Gauss		ADF	ADF	Gauss	ADF	ADF	Gauss
method:		DFT	DFT	DFT		DFT	DFT	DFT	DFT	DFT	DFT
functional:		PW91	OLYP	B3LYP		PW91	OLYP	B3LYP	PW91	OLYP	B3LYP
basis set:	X-ray	ZORA/TZP	ZORA/TZP	CEP-31G	X-ray	ZORA/TZP	ZORA/TZP	CEP-31G	ZORA/TZP	ZORA/TZP	CEP-31G
rmsd		0.06	0.09	0.10		0.11	0.12	0.34			
Bond Lengths/Å											
Hg1−S1	2.389	2.430	2.422	2.508	2.372	2.425	2.412	2.498	2.403	2.399	2.470
Hg1−C2	2.058	2.116	2.116	2.149	2.101	2.099	2.099	2.125	2.100	2.101	2.126
Hg1−N1	2.577	2.617	2.753	2.600	2.651	2.617	2.777	2.592	2.671	2.825	2.672
N1−N2	1.276	1.277	1.273	1.308	1.277	1.276	1.272	1.307	1.283	1.279	1.311
N1−C8	1.438	1.412	1.418	1.444	1.432	1.412	1.418	1.444	1.405	1.411	1.438
N2−C1	1.409	1.369	1.375	1.400	1.416	1.370	1.375	1.400	1.366	1.368	1.399
C1−S1	1.749	1.783	1.783	1.855	1.731	1.785	1.786	1.857	1.780	1.785	1.848
C1−N3	1.304	1.327	1.325	1.342	1.301	1.325	1.324	1.341	1.332	1.331	1.343
N3−N4	1.326	1.317	1.315	1.353	1.337	1.318	1.316	1.353	1.319	1.317	1.356
N4−C14	1.406	1.396	1.399	1.424	1.401	1.397	1.399	1.425	1.391	1.393	1.422
Bond Angles/deg											
Hg1−S1−C1	104.8	102.7	104.7	101.0	104.8	102.1	104.4	100.9	102.5	104.4	101.6
S1−Hg1−N1	74.1	74.6	73.3	75.7	73.8	74.6	73.1	76.0	75.1	73.5	76.2
N1−Hg1−C2	119.4	118.6	117.2	120.5	118.4	119.9	117.4	120.8	115.6	113.5	115.5
Hg1−N1−N2	119.5	117.2	114.7	118.7	115.1	116.6	113.7	118.5	114.2	111.5	115.7
N1−N2−C1	115.6	118.1	118.9	118.5	117.7	118.2	118.9	118.6	119.0	119.8	119.2
N2−C1−S1	125.8	127.1	128.0	126.0	124.8	126.8	127.8	125.9	128.1	129.1	127.3
S1−C1−N3	123.1	121.2	121.6	122.2	127.5	121.4	121.5	122.2	114.5	113.4	115.0
C1−N3−N4	116.4	117.3	118.8	118.5	116.0	117.5	118.8	118.6	117.6	118.3	119.7

[a] The root-mean-square deviations (rmsd) of computed structures are given.

example, the calculated Hg−Hg distance of Hg_2^{2+} using ADF/ZORA/TZ2P with the BPW91 exchange/correlation functional is 2.70 Å in the gas phase. In aqueous solution (dielectric constant = 78.4), the calculated Hg−Hg distance decreases by 0.18 Å to a value of 2.52 Å.[25] The Hg−Hg distance of Hg_2^{2+} in solution is known from EXAFS studies to be 2.52 Å,[26] while the typical value within crystals is 2.50(1) Å.[27]

Similarly, but with the exception of the Hg−C2 (ADF) and Hg−N1 (ADF/PW91 and G03/B3LYP) bonds in the PhHgHDz (orange) optimization alone, all other calculated gas-phase Hg−ligand bonds were found to be slightly longer than the corresponding solid state bond lengths from crystal data. The ADF/OLYP optimization of PhHg(cptsc) gave simultaneously the largest and smallest bond length deviations, namely, 0.222

Å (Hg−N1) and 0.032 Å (Hg−S) respectively. G03 (B3LYP) tends to give calculated Hg−S bonds more than 0.1 Å longer than corresponding X-ray determined distances. ADF/OLYP consistently gave Hg−N bond distances 0.12 up to 0.18 Å too long. With the exception of the ADF/OLYP calculations of Hg−N bond distances then, lengthening of metal-centered bonds in all the gas-phase calculations of this study are not as pronounced as in the formerly mentioned Hg−Hg bond distances. Unfortunately no previously calculated Hg−S or Hg−N bond distances could be found in the published literature.

The ADF/PW91 calculated Hg−C2 bond (2.099 Å) of the PhHgHDz (orange) structure is for all practical purposes similar in length to that found in the crystal structure (2.101 Å). The Hg−N1 bond, however, was found to be 0.034 (ADF/PW91) and 0.059 Å (G03/B3LYP) shorter. In the MeHgHDz structure which is largely similar to PhHgHDz except for the different R-group *trans* to the dithizonato ligand, the Hg−N1 bond is, on the contrary, 0.040 (ADF/PW91) and 0.023 (G03/B3LYP) Å *longer* than in the crystal structure. Since the Hg−N1 bond length deviations are relatively small (0.059 Å or less) compared to the experimental bond itself (2.651 Å), i.e. the true bond length could be approached within 97.8%, we consider the calculation to be of high accuracy.

A comparison between ADF/PW91 calculations which took relativistic effects into account (as generally done in this study) and nonrelativistic calculations resulted in Hg−S1 and Hg−C2 bond length decreases of 0.113 and 0.092 Å respectively, and the Hg−N1 bond length increasing by 0.116 Å, all in favor of experimental bond lengths (see Supporting Information, Table S3). Solvent-effects on the calculated equilibrium bond lengths and angles were modest, as expected for neutral molecules.[24] (Supporting Information, Table S2)

The calculated C−N and N−N bond lengths in the ligand backbones of all the molecules here investigated were found to deviate by not more than *ca.* ±0.05 Å (<4%) from crystallographic data. The high degree of electron delocalization along the dithizonato backbone is emphasized by the following computed results and observations: In general, typical C−N single and double bond distances are 1.47 and 1.29 Å, while N−N single and double bonds are 1.45 and 1.25 Å.[28] In the ADF structure of PhHgHDz (orange isomer) the N1═N2 double bond is 1.276 Å (X-ray: 1.277 Å), N2−C1 is 1.370 Å (X-ray: 1.416 Å), C1═N3 is 1.325 Å (X-ray: 1.301 Å) and N3−N4 is 1.318 Å (X-ray: 1.337 Å). All these values lie in between typical single and double bond distance values. The N−phenyl bond lengths, being on average 1.405 Å, are also shorter than the typical C−N single bond length of 1.47 Å. The aromatic phenyl rings are thus included in the conjugation pattern that spans along the full length of the ligand.

Bond angles, especially in the thiosemicarbazonato complexes, closely agree with crystallographic data. They varied by only *ca.* 0−4° from crystal structure values. The S−C1−N3 angle in the PhHgHDz molecule is the only exception, being 4.8 to 6.1° smaller than the corresponding crystal structure angle in all three computational approaches. With fewer movement restrictions around the C1−N3 bond, and the possibility of packing effects in the crystal, this result is not rejected, but attributed to typical gas-phase calculation results.

Side views of selected optimized geometries and the crystal structure of PhHgHDz are shown in Figure 2. As in the crystal structure (view a), both pure density functional methods, ADF/PW91 (view b) and OLYP (not shown) resulted in a bent dithizonato backbone. The Gaussian hybrid functional B3LYP (which has 20% Hartree−Fock exchange)[29] optimized the molecule to a strictly planar geometry, see view (c) for G03/B3LYP, despite imposing no symmetry limitations on the calculation. The DFT method as employed in the Amsterdam Density Functional program package therefore gives a better reflection of the experimental geometry. The bent geometry observed in the X-ray structure determination of PhHgHDz (orange form) might have been attributed to packing effects, but since, in contrast, both the **Me**HgHDz crystal and ADF structures are planar in turn (see Supporting Information, Figure S2), the bent conformation appears to be at least partially also the consequence of intramolecular electronic effects. The clear difference between PhHgHDz and MeHgHDz planarity supports the notion that the *degree* of planarity of the RHgHDz molecule is affected by the potential of the R-group *trans* to the dithizonato ligand, to donate or withdraw electron density to or from the rest of the molecule.

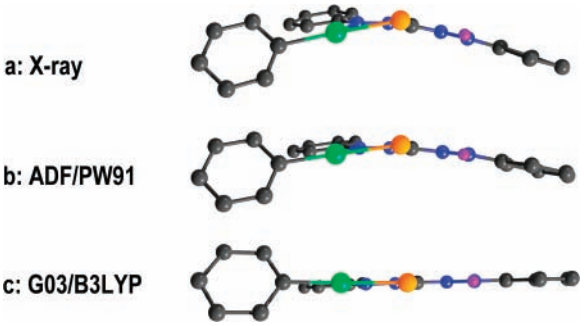

Figure 2. Side perspectives of the orange isomer of PhHgHDz, comparing the (a) X-ray determined structure to (b) ADF/PW91, and (c) G03/B3LYP calculated geometries. Phenyl hydrogens are omitted. (Key: green, Hg; orange, S; blue, N; violet, H; gray, C.)

The phenyl ring bonded to the Hg atom in PhHgHDz (orange isomer) was found to be almost perpendicular to the ligand plane, Figure 2. In contrast, the phenyl rings of the dithizonato ligand are both coplanar with the ligand backbone. This observation is in agreement with the N−phenyl conjugated bonds discussed earlier, indicating a high degree of conjugation between the phenyl rings and adjacent nitrogens in the dithizonato Ph−N−N−C−N−N−Ph backbone. Phenyl π-orbitals are therefore expected to overlap with adjacent unhybridized nitrogen p-orbitals directed vertically to the ligand plane.

From the above-described structural comparisons it is clear that ADF calculations mostly repeated experimentally determined structural results at a *ca.* 97% level and higher. Only the S−C1−N3 bond angle deviates by 5% from experimental values. As may further be seen from Tables 1 and 2, the methods that gave the smallest root-mean-square deviations from the crystal structures, and therefore the closest representation of experimental structural data, are the methods that included the PW91 and OLYP functionals. The hybrid functional B3LYP performed the poorest, especially in describing PhHgHDz (orange isomer). The largely planar optimized G03/B3LYP geometry explains the large rmsd value of 0.34.

Structure of the Blue Isomer. Having convincingly proved that density functional theory can accurately predict ground state structures of mercury dithizonate complexes, our attention was refocused on efforts to predict with confidence the unknown structure of the photoexcited blue mercury dithizonate isomer. The intuitively predicted structure that was favored to date is presented in Scheme 1. Figure 3a also shows the same structure, which will henceforth be referred to as structure N2H. Two other alternatives, S1H (Figure 3b) and N4H (Figure 3c), are also indicated. A dithizonato proton is bonded to N4 in configuration N4H. The main difference between the proposed structure N4H

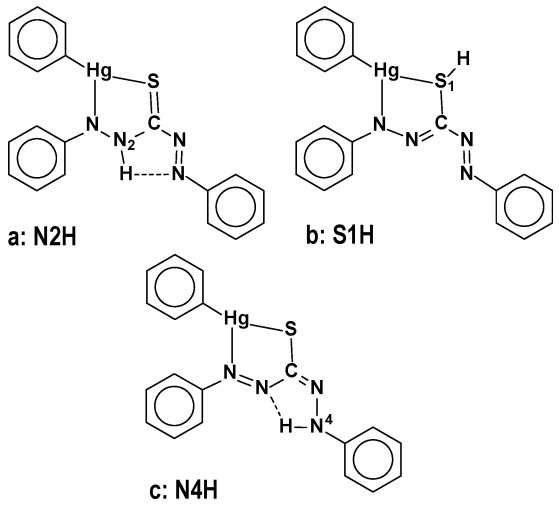

Figure 3. Different investigated structural geometries for the *blue* isomer of PhHgHDz: (a) N2H, (b) S1H and (c) N4H.

TABLE 3: Energies of the Lowest Energy Optimized Blue Form Structures of PhHgHDz Relative to That of the Orange Isomer

PhHgHDz	ADF/PW91 /ZORA/TZP/ (kJ mol^{-1})	ADF/OLYP/ ZORA/TZP/ (kJ mol^{-1})	G03/B3LYP/ CEP-31G (kJ mol^{-1})
structure N4H	24.4	23.3	20.5
structure N2H	60.1	60.8	68.0
structure S1H	110.3	100.5	166.7

and structure N2H is that the dithizonato proton stays intact on N4 throughout the reversible photochromic reaction, and is not intra- or intermolecularly transferred as earlier speculated (Scheme 1).

Of the three different PhHgHDz blue form models studied, the S1H structure is the least likely, because it has the highest energy relative to that of the orange isomer, see Table 3. Structure N2H, most widely supported by previous researchers,[4,5] has the second highest energy, while the energy of structure N4H is the lowest, being 35.7 kJ·mol^{-1} (ADF/PW91), 37.5 kJ·mol^{-1} (ADF/OLYP) and 47.5 kJ·mol^{-1} (G03/B3LYP) less than the N2H structure. In addition, all the energy differences between the N4H and N2H geometries are significantly larger (>35 kJ·mol^{-1}) than the energy differences between the orange ground state isomer and the photoexcited N4H blue isomer (<25 kJ·mol^{-1}). Energetically therefore, and unlike previous expectations, the N4H configuration of the blue excited state isomer (Figure 3c) represents the most favorable computed geometry within the series of possible structures studied here. Solvent effects were also investigated, but the effect on the relative stability of the different PhHgHDz isomers was found to be minimal (See Supporting Information, Table S2).

Due to the fact that ADF/PW91 gave the smallest root-mean-square deviation from crystal data (0.11) for the orange isomer, the ADF density functional PW91 method is believed to give the most reliable geometry prediction of the hitherto unknown structure of the blue isomeric form of dithizonatophenylmercury-(II).

Bond distances and angles for the proposed N4H structure are summarized in Table 2. The slightly bent conformation of the blue isomer, as seen in Figure 4a, is favored over the linear structure computed via the G03/B3LYP route, because it parallels that of the orange isomer, Figure 2b. As in the orange isomer, the Hg−phenyl lies again almost perpendicular to the plane of the dithizonato ligand.

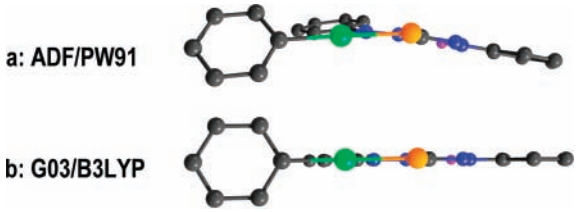

Figure 4. Side perspectives of the N4H blue isomer of PhHgHDz, comparing computational results of the different basis sets: (a) ADF/ZORA/TZP/PW91 and (b) G03/B3LYP/CEP-31G. Phenyl hydrogens are omitted. (Key: green, Hg; orange, S; blue, N; violet, H; gray, C.)

TABLE 4: Experimental and Calculated Excitation Energies (Expressed as Wavelength λ) and Oscillator Strengths (f, in au = Atomic Units, Indicating Relative Oscillator Absorption Strength as a Number) for the Strongest Optically Allowed States of the Orange Isomer of PhHgHDz Compared to the Experimental Electronic Spectrum in Hexane Solution

experimental		ADF/PW91/ ZORA/TZP		ADF/OLYP/ ZORA/TZP		Gaussian/B3LYP/ CEP-31G	
λ/nm	relative absorbance	λ/nm	f/au	λ/nm	f/au	λ/nm	f/au
471	0.84	508	0.446	504	0.270	474	0.566
		502	0.075	492	0.297	472	0.154
422	0.39	422	0.321	409	0.292	385	0.203
342	0.07	349	0.065	348	0.060	321	0.090
300	0.23	295	0.175	296	0.147	270	0.070
265	0.48	286	0.081	282	0.136	262	0.092
		285	0.095				

TABLE 5: Experimental and Selected Calculated Excitation Energies (Expressed as Wavelength λ) for the Strongest Oscillator Peaks (f) of the Two Blue Forms of PhHgHDz, N4H and N2H

	experimental		ADF/PW91/ ZORA/TZP		Gaussian/B3LYP/ CEP-31G	
	λ/nm	relative absorbance	λ/nm	f/au	λ/nm	f/au
blue N4H	604	0.41	738	0.165	623	0.298
			482	0.114	432	0.291
			468	0.175		
	367	0.33	367	0.141	334	0.184
	310	0.13	321	0.114	288	0.082
	275	0.58	305	0.300	283	0.083
blue N2H	604	0.41	664	0.314	631	0.365
			421	0.158		
	367	0.33	316	0.468	382	0.327
	310	0.13			303	0.151
	275	0.58			284	0.279

A similar high degree of conjugation extending along the entire ligand backbone as discussed for the orange isomer is observed for the blue N4H isomer. Except for the ADF/PW91 optimized Hg−S bond being 0.022 Å shorter and the Hg−N1 bond being 0.054 Å longer than in the orange isomer, other bond distances do not differ more than 0.007 Å. The S−C1−N3 bond angle has the largest deviation, namely, 6.9° smaller than in the orange structure. Rotation around the C1−N3 bond of the orange isomer, caused by photoexcitation, results in a decrease of the S−C1−N3 bond angle from 121.4° in the orange isomer to 114.5° in the N4H blue isomer.

With the N4-H hydrogen atom being in relatively close proximity to S (orange isomer) and N2 (blue isomer), the possibility of varied strength intramolecular hydrogen bonds inevitably has to be considered. Due to the inability of DFT to calculate these hydrogen bond strengths, the classification provided by Jeffrey, based on positional parameters, was

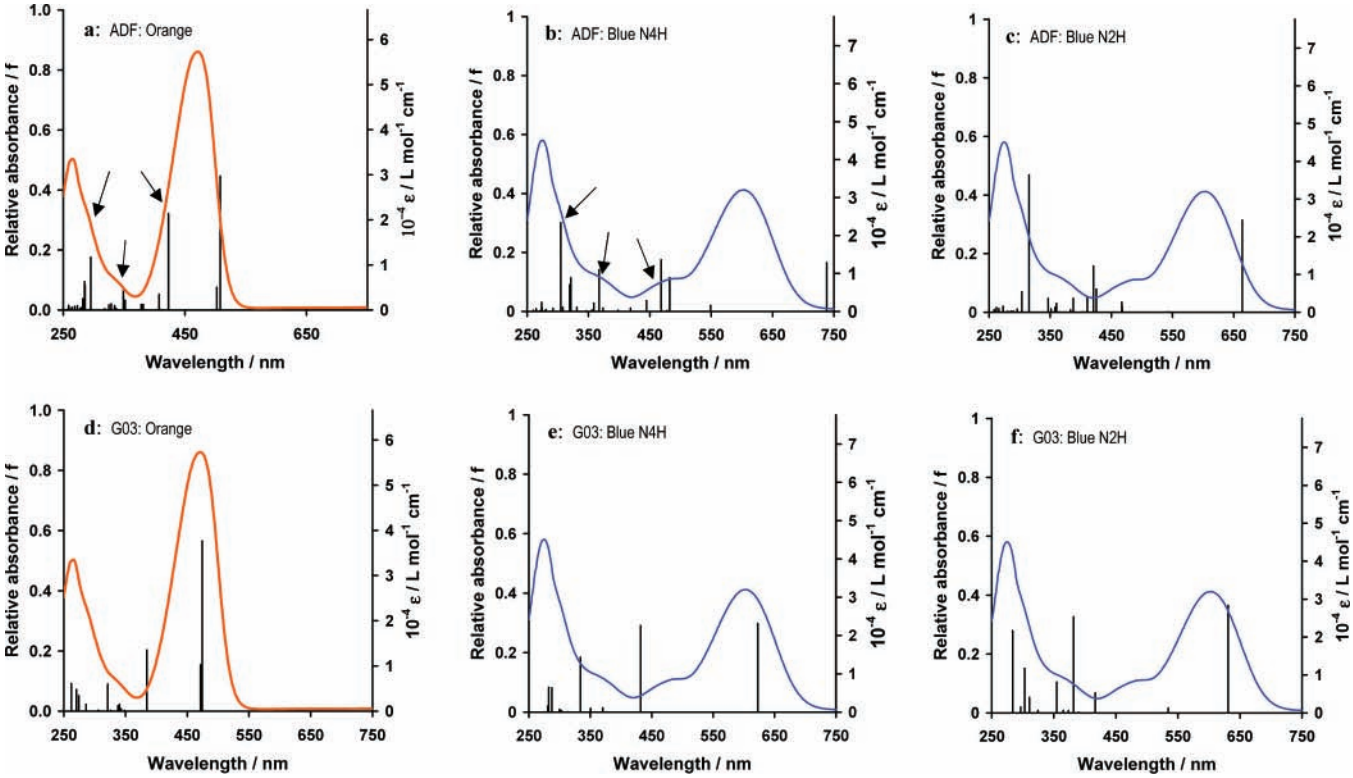

Figure 5. ADF (a, b and c) and G03/B3LYP (d, e and f) calculated electronic spectra (bars) and experimental spectra in hexane (lines) of the isomers of PhHgHDz. Left: Orange isomer. Middle: Blue isomer, structure N4H. Right: Blue isomer, structure N2H. Both the N4H (middle) and N2H (right) oscillators are overlaid with the same experimental blue spectrum. General: *Y*-axis gives relative absorbance for experimentally determined spectra and f = atomic units for calculated oscillator strengths. Arrows indicate shoulders to the main peaks.

employed as a useful guide instead.[30] He categorized hydrogen bond lengths of 1.5−2.2 Å as representative of moderate strength hydrogen bonds, bond lengths >2.2 Å are associated with weak hydrogen bonds, bond angles >130° are typical of moderate strength hydrogen bonds, and bond angles >90° are associated with weak hydrogen bonds. The ADF optimized structure results in an N4-H−N2 hydrogen bond distance in the blue isomer of 2.13 Å, which classifies it as of moderate strength, based on bond distance alone. The N4−H−N2 bond angle of 103.4°, however, lies in the category of weak hydrogen bonding. The orange isomer N4-H−S hydrogen bond length (2.34 Å) and angle (111.7°) are both indicative of a weak hydrogen bond. Additionally, S−H hydrogen bonds are known to be significantly weaker than N−H hydrogen bonds, e.g., calculated bond energies in gas-phase dimers were found to be 4.6 kJ·mol^{-1} for the S−H−S type, and 100 kJ·mol^{-1} for the N−H−N type.[30] It is therefore concluded that intramolecular hydrogen bonding might not be playing a significant role in the stability of especially the ground state orange isomer. Its weakness is consistent with it not preventing the conformational change from the orange to the blue form upon photoexcitation. Once the conformational change has taken place, though, it seems appropriate that it may assist in retarding the back reaction of the photoexcited blue isomer when the light source is removed. The relatively long lifetimes ($t_{1/2}$ > 60 s in DCM) typically observed for the blue N4H complex are mutually consistent with such an assumption. Other metal dithizonato complexes, however, revert back much faster to the resting ground state.[4]

Electronic Spectra. In an attempt to correlate the orange structure of PhHgHDz and the possible blue N4H or N2H photoexcited forms of PhHgHDz with experimentally observed UV/visible spectra of the blue and orange forms of PhHgHDz, we proceeded to theoretically calculate the UV/visible spectra of these three forms of PhHgHDz. The visible region of the experimental spectrum of the orange isomer is dominated by a relatively intense asymmetric band with λ_{max} = 471 nm (ϵ = 57 300 dm^3 mol^{-1} cm^{-1}). The asymmetric shape of this band may be attributed to the superposition of a number of individual bands.[31] The near-UV region of the spectrum is characterized by a broad band of overlapping peaks with λ_{max} = 265 nm (ϵ = 32 200 dm^3 mol^{-1} cm^{-1}) and two shoulders at *ca.* 295 and 340 nm. The trough between the two maxima lies at 369 nm. Since the absorption is not zero here, as for λ > 570 nm, some absorption oscillators should be evident from a theoretical calculation, even at this minimum.

Computed energies underlying the experimental UV/visible spectra of the different isomers of PhHgHDz are reported in Tables 4 and 5. Selected examples of calculated electronic absorption spectra of the orange and blue isomers (both the N4H and N2H configurations) of PhHgHDz are given in Figure 5. Experimental spectra are superimposed onto the calculated spectral oscillators shown as bars.

The ADF/PW91, ADF/OLYP (not shown) and G03/B3LYP theoretical spectra for the orange isomer of PhHgHDz show a pattern similar to the experimental UV/vis results, even though the peaks do not match exactly, see Table 4 and Figure 5, left. At shorter wavelengths, up to 422 nm, the ADF calculations produced optical absorption oscillators that coincide closely with experimentally observed peaks and shoulders, with the biggest deviation being at 265 nm (experimental), versus 286 nm (ADF/PW91). The two longest wavelength calculated signals which appear at 472 and 474 nm (G03/B3LYP), and 502 and 508 nm (ADF/PW91) in the visible region, are mainly attributed to transitions from the HOMO−1 to LUMO and HOMO to LUMO respectively. These peaks correspond to the experimental maximum at 471 nm, with G03/B3LYP giving an exceptionally good approximation here. The third lowest energy ADF/PW91

calculated peak (423 nm), attributed to the HOMO−3 to LUMO transition, appears to match an unresolved experimental peak at *ca.* 422 nm. This peak is observed as a slight shoulder on the experimental spectrum. Even the observed minimum at 369 nm is well reproduced by the calculated spectra.

The experimental UV/visible spectrum of the blue photoexcited state of PhHgHDz also shows two dominant peaks. Maxima are observed at 275 nm ($\epsilon = 37\,650$ dm^3 mol^{-1} cm^{-1}) and 604 nm ($\epsilon = 26\,000$ dm^3 mol^{-1} cm^{-1}) with a minimum lying at *ca.* 415 nm, as shown by the solid line spectrum of Figure 5, middle and right. The small shoulder that appears at 450−490 nm on the experimental spectrum of the blue form is the result of partial back conversion to the orange ground state and is therefore not uniquely part of the blue isomer spectrum.

Both the experimental minimum at 415 nm and the shoulders lying below this minimum are well reproduced by the ADF/PW91 calculation of the N4H blue isomer, with peaks at 321 nm (experimental: 310 nm) and 367 nm (experimental: 370 nm) respectively. The calculated maximum at 305 nm corresponds to the experimental maximum at 275 nm. ADF/PW91, however, fails to predict the experimental maximum at 604 nm correctly. The same features found for the calculated ADF/PW91 N4H spectrum are found for the calculated ADF/OLYP N4H spectrum (see Supporting Information, Table S6). In contrast, the G03/B3LYP theoretical spectrum of the N4H blue isomer of PhHgHDz predicts the lowest energy maximum at 623 nm (experimental: 604 nm), but the relative intensities of the peaks at 334 and 432 nm do not match the experimental spectrum in this case. The general features and relative intensities of the calculated spectrum of the N2H blue isomer of PhHgHDz do not match the experimental blue spectrum as well as in the case of N4H. Differences between the experimental and calculated spectra are especially noticeable in the region of the experimental minimum of 415 nm where strong calculated oscillators are observed.

The present study cannot exclude the possibility that a tautomeric equilibrium exists between the N4H and N2H blue tautomers in solution, similar to the keto−enol tautomery of beta-diketones in solution.[32] However, since the calculated blue N4H spectra give a better description of the observed experimental spectrum, it will most probably be the dominant species in solution.

The Gaussian/B3LYP results were surprising in that not only did the peak positions of the longer wavelength peak at $\lambda =$ 474 nm (orange isomer) and 623 nm (N4H blue isomer) coincide with the experimental UV/visible absorbance bands but also relative intensities corresponded very closely to experiment. The ratio of the strongest oscillator strength of the orange isomer (0.57, 474 nm) to the corresponding value for the N4H blue isomer (0.30, 623 nm) is 1.90. Comparing experimental molar absorptivities similarly gave a ratio of *ca.* 2.15. For the N2H blue isomer the ratio is 1.55.

4. Conclusion

Quantum computational data, having utilized both the Amsterdam Density Functional and Gaussian programs, are mutually consistent in predicting the orange isomer of dithizonatophenylmercury(II) to be the naturally occurring stable form. The ADF-2006 package with the PW91 functional gave the closest approximation of the molecular structure of the orange isomer, and with this evidence extrapolated the most likely structure of the blue isomer could be predicted. Geometry optimization data and calculated molecular energies support a structure for the photoexcited blue isomer without intramolecular proton transfer, i.e., the backbone proton remains intact on the N4 position. General tendencies in the calculated electronic spectra for the newly predicted N4H structure are mutually consistent with experimental spectra, with the Gaussian/B3LYP program giving the best approximation of the HOMO to LUMO excitation in both isomers.

Acknowledgment. The National Research Foundation of South Africa (Grant 2054243) and the Central Research Fund of the University of the Free State, Bloemfontein, are gratefully acknowledged.

Supporting Information Available: Additional figure and tables as described in the text. This information is available free of charge via the Internet at http://pubs.acs.org.

References and Notes

(1) Reith, J. F.; Gerritsma, K. W. *Recl. Trav. Chim. Pays-Bas* **1945**, *64*, 41.

(2) Irving, H. M. N. H.; Andrew, G.; Risdon, E. J. *J. Chem. Soc*. **1949**, 541.

(3) Webb, J. L. A.; Bhatia, I. S.; Corwin, A. H.; Sharp, A. G. *J. Am. Chem. Soc*. **1950**, *72*, 91.

(4) Meriwether, L. S.; Breitner, E. C.; Sloan, C. L. *J. Am. Chem. Soc*. **1965**, *87*, 4441.

(5) (a) Bouas-Laurent, H.; Dürr, H. *Pure Appl. Chem*. **2001**, *73*, 639−665. (b) Hutton, A. T.; Irving, H. M. N. H. *J. Chem. Soc., Dalton Trans*. **1982**, 2299.

(6) Hutton, A. T.; Irving, H. M. N. H.; Nassimbeni, L. R. *Acta Crystallogr*. **1980**, *B36*, 2064.

(7) Meriwether, L. S.; Breitner, E. C.; Colthup, N. B. *J. Am. Chem. Soc*. **1965**, *87*, 4448.

(8) (a) Foster, W. H.; Dowd, J. M.; Coleman, R. A. U.S. Patent 3,475,339; *Chem. Abstr*. **1970**, *72*, 56633n. (b) Kazan, J.; Foster, W. H. U.S. Patent 3,505,306; *Chem. Abstr*. **1970**, *73*, 46684m. (c) Shimano, Y.; Jpn. Patent 70 50 355; *Chem. Abstr*. **1974**, *80*, 97349h.

(9) Velde, G. T.; Bickelhaupt, F. M.; Baerends, E. J.; Guerra, C. F.; Van Gisbergen, S. J. A.; Snijders, J. G.; Ziegler, T. J. *J. Comput. Chem*. **2001**, *22*, 931−967.

(10) Perdew, J. P.; Chevary, J. A.; Vosko, S. H.; Jackson, K. A.; Perderson, M. R.; Singh, D. J.; Fioihais, C. *Phys. Rev*. **1992**, *B46*, 6671−6687.

(11) Handy, N. C.; Cohen, A. *J. Mol. Phys*. **2001**, *99*, 403−412.

(12) (a) Lee, C.; Yang, W.; Parr, R. G. *Phys. Rev*. **1988**, *B37*, 785. (b) Miehlich, B.; Savin, A.; Stoll, H.; Preuss, H. *Chem. Phys. Lett*. **1989**, *157*, 200.

(13) Van Lenthe, E.; Ehlers, A. E.; Baerends, E. J. Geometry optimization in the Zero Order Regular Approximation for relativistic effects. *J. Chem. Phys*. **1999**, *110*, 8943−8953.

(14) Van Gisbergen, S. J. A.; Snijders, J. G.; Baerends, E. J. *Comput. Phys. Commun*. **1999**, *118*, 119−138.

(15) (a) Klamt, A.; Schüürmann, G. *J. Chem. Soc., Perkin Trans*. **1993**, *2*, 799−805. (b) Klamt, A. *J. Phys. Chem*. **1995**, *99*, 2224−2235. (c) Klamt, A.; Jonas, V. *J. Chem. Phys*. **1996**, *105*, 9972−9980.

(16) Pye, C. C.; Ziegler, T. *Theor. Chem. Acc*. **1999**, *101*, 396−408.

(17) Frisch, M. J.; Trucks, G. W.; Schlegel, H. B.; Scuseria, G. E.; Robb, M. A.; Cheeseman, J. R.; Montgomery, J. A., Jr.; Vreven, T.; Kudin, K. N.; Burant, J. C.; Millam, J. M.; Iyengar, S. S.; Tomasi, J.; Barone, V.; Mennucci, B.; Cossi, M.; Scalmani, G.; Rega, N.; Petersson, G. A.; Nakatsuji, H.; Hada, M.; Ehara, M.; Toyota, K.; Fukuda, R.; Hasegawa, J.; Ishida, M.; Nakajima, T.; Honda, Y.; Kitao, O.; Nakai, H.; Klene, M.; Li, X.; Knox, J. E.; Hratchian, H. P.; Cross, J. B.; Bakken, V.; Adamo, C.; Jaramillo, J.; Gomperts, R.; Stratmann, R. E.; Yazyev, O.; Austin, A. J.; Cammi, R.; Pomelli, C.; Ochterski, J. W.; Ayala, P. Y.; Morokuma, K.; Voth, G. A.; Salvador, P.; Dannenberg, J. J.; Zakrzewski, V. G.; Dapprich, S.; Daniels, A. D.; Strain, M. C.; Farkas, O.; Malick, D. K.; Rabuck, A. D.; Raghavachari, K.; Foresman, J. B.; Ortiz, J. V.; Cui, Q.; Baboul, A. G.; Clifford, S.; Cioslowski, J.; Stefanov, B. B.; Liu, G.; Liashenko, A.; Piskorz, P.; Komaromi, I.; Martin, R. L.; Fox, D. J.; Keith, T.; Al-Laham, M. A.; Peng, C. Y.; Nanayakkara, A.; Challacombe, M.; Gill, P. M. W.; Johnson, B.; Chen, W.; Wong, M. W.; Gonzalez, C.; Pople, J. A. *Gaussian 03*, Revision C.02; Gaussian, Inc.: Wallingford, CT, 2004.

(18) (a) Stephens, P. J.; Devlin, F. J.; Chabalowski, C. F.; Frisch, M. J. *J. Phys. Chem*. **1994**, *98*, 11623−11627. (b) Watson, A.; Handy, N. C.; Cohen, A. J. *J. Chem. Phys*. **2003**, *119*, 6475−6481. (c) Hertwig, R. H.; Koch, W. *Chem. Phys. Lett*. **1997**, *268*, 345−351.

(19) (a) Stevens, W.; Basch, H.; Krauss, J. *J. Chem. Phys.* **1984**, *81*, 6026. (b) Stevens, W. J.; Krauss, M.; Basch, H.; Jasien, P. G. *Can. J. Chem.* **1992**, *70*, 612. (c) Cundari, T. R.; Stevens, W. J. *J. Chem. Phys.* **1993**, *98*, 5555.

(20) (a) Stratmann, R. E.; Scuseria, G. E.; Frisch, M. J. *J. Chem. Phys.* **1998**, *109*, 8218. (b) Bauernschmitt, R. and Ahlrichs, R. *Chem. Phys. Lett.* **1996**, *256*, 454. (c) Casida, M. E.; Jamorski, C.; Casida, K. C.; Salahub, D. R. *J. Chem. Phys.* **1998**, *108*, 4439.

(21) Zhurko, G. A.; Zhurko, D. A. *Chem Craft*, version 1.5 (build 275); 2007.

(22) Zukermanschpector, J.; Rodriguezarguelles, M. C.; Suarez, M. I.; Sanchez, A.; Casas, J. S.; Sordo, J. *J. Coord. Chem.* **1991**, *24*, 177−181.

(23) Lobana, T. S.; Sanchez, A.; Casas, J. S.; Castineiras, A.; J. Sordo, Garcia-Tasende, M. S.; Vazquez-Lopez, E. M. *J. Chem. Soc., Dalton Trans.* **1997**, 4289−4299.

(24) Hehre, W. J. *A Guide to Molecular Mechanisms and Quantum Chemical Calculations*; Wavefunction Inc.: Irvine, CA, 2003; pp 153, 181.

(25) McKee, M. L.; Swart, M. *Inorg. Chem.* **2005**, *44* (20), 6975.

(26) Rosdahl, J.; Persson, I.; Kloo, L.; Ståhl, K. *Inorg. Chim. Acta* **2004**, *357*, 2624.

(27) Sikirica, M.; Grdenic, D. *Acta Crystallogr., Sect. B* **1974**, *B30*, 144.

(28) *Cambridge Structural Database (CSD)*, version 5.27; 2006. Allen, F. H. *Acta Crystallogr.* **2002**, *B58*, 380−388.

(29) Becke, A. D. *J. Chem. Phys.*, **1993**, *98*, 5648.

(30) (a) Jeffrey, G. A. *An Introduction to Hydrogen Bonding*; Oxford University Press: Oxford, 1997. (b) Steiner, T. *Angew. Chem., Int. Ed.* **2002**, *41*, 48−76.

(31) Tovbin, Y. K.; Romm, I. P.; Ostrovskii, G. M.; Gur'yanova, E. N. *J. Appl. Spectrosc.* **1975**, *22*, 362−365.

(32) du Plessis, W. C.; Davis, W. L.; Cronje, S. J.; Swarts J. C. *Inorg. Chim. Acta* **2001**, *314*, 97−104.